PCCP

PAPER

View Article Online
View Journal | View Issue

Cite this: *Phys. Chem. Chem. Phys.*, 2015, **17**, 22736

Influence of the sterol aliphatic side chain on membrane properties: a molecular dynamics study†

João R. Robalo,[ab] J. P. Prates Ramalho,[a] Daniel Huster*[c] and Luís M. S. Loura*[de]

Received 28th May 2015,
Accepted 31st July 2015

DOI: 10.1039/c5cp03097h

www.rsc.org/pccp

Following a recent experimental investigation of the effect of the length of the alkyl side chain in a series of cholesterol analogues (*Angew. Chem., Int. Ed.*, 2013, **52**, 12848–12851), we report here an atomistic molecular dynamics characterization of the behaviour of methyl-branched side chain sterols (iso series) in POPC bilayers. The studied sterols included androstenol (i-C0-sterol) and cholesterol (i-C8-sterol), as well as four other derivatives (i-C5, i-C10, i-C12 and i-C14-sterol). For each sterol, both subtle local effects and more substantial differential alterations of membrane properties along the iso series were investigated. The location and orientation of the tetracyclic ring system is almost identical in all compounds. Among all the studied sterols, cholesterol is the sterol that presents the best matching with the hydrophobic length of POPC acyl chains, whereas longer-chained sterols interdigitate into the opposing membrane leaflet. In accordance with the experimental observations, a maximal ordering effect is observed for intermediate sterol chain length (i-C5, cholesterol, i-C10). Only for these sterols a preferential interaction with the saturated *sn*-1 chain of POPC (compared to the unsaturated *sn*-2 chain) was observed, but not for either shorter or longer-chained derivatives. This work highlights the importance of the sterol alkyl chain in the modulation of membrane properties and lateral organization in biological membranes.

Introduction

Cholesterol is usually the most abundant single molecular lipid species in mammalian membranes, comprising up to 45 mol% of the total lipid.[1] It is the essential component for maintaining the barrier function of the membrane and plays a crucial role in the lateral organization of the membrane lipids, the dynamic domain structure and the elasticity of the membrane that is required for membrane protein function.[2–4] These and other important membrane properties come about by specific interactions between cholesterol and other lipids or proteins in the membrane.[5,6] So far, little has been understood about these specific interactions, and exact interaction energies that would allow understanding the lateral organization of lipids and proteins in the membrane have only been estimated. Evidence has accumulated that cholesterol likes to interact with saturated lipid chains while contacts with unsaturated chains are less favored.[1,7,8] Due to favorable van der Waals interactions between the tetracyclic ring system of cholesterol and also the cholesterol side chain, the saturated chains of phospholipids are ordered, which decreases the area per lipid molecule, a phenomenon referred to as condensation.[9] This leads to a denser packing of the lipids and consequently reduces the permeability of the membrane for polar and unipolar molecules.

It is widely accepted that the sterol tetracyclic ring system is a major structural determinant of the effects of these molecules on membrane physical properties. Molecular dynamics simulations (MD) showed that alterations in the ring substituents of cholesterol lead to a reduction of the cholesterol specific condensation effect on the membrane phospholipids indicated by increased cross-sectional areas per lipid molecule and lower deuterium order parameter profiles of their acyl chains.[10] These changes were accompanied by higher average values of the tilt of the sterol long axis relative to the membrane normal (θ), which led the authors of this work to propose this parameter as an indicator of its capability of ordering phospholipid bilayers. This tilt effect may be explained by a thermodynamical formulation in terms of

[a] *Centro de Química de Évora and Departamento de Química, Escola de Ciências e Tecnologia, Universidade de Évora, P-7000-671 Évora, Portugal*
[b] *Theory and Bio-Systems Department, Max Planck Institute of Colloids and Interfaces, Wissenschaftspark Golm, D-14424 Potsdam, Germany*
[c] *Institute of Medical Physics and Biophysics, University of Leipzig, Härtelstr. 16-18, D-04107 Leipzig, Germany. E-mail: daniel.huster@medizin.uni-leipzig.de; Fax: +49 (0)341 97 15709; Tel: +49 (0)341 97 15700*
[d] *Centro de Química de Coimbra, Largo D. Dinis, Rua Larga, P-3004-535 Coimbra, Portugal*
[e] *Faculdade de Farmácia, Universidade de Coimbra, Pólo das Ciências da Saúde, Azinhaga de Santa Comba, P-3000-548 Coimbra, Portugal. E-mail: lloura@ff.uc.pt; Fax: +351 239827126; Tel: +351 239488485*

† Electronic supplementary information (ESI) available. See DOI: 10.1039/c5cp03097h

a tilt modulus, which quantifies the energetic cost of tilting sterol molecules inside the membrane.[11] Róg *et al.*[12] reviewed data from both experimental and MD studies of lipid mixtures containing cholesterol or other sterols along the cholesterol biosynthetic pathway (*e.g.* lanosterol, desmosterol, and 7-dehydrocholesterol), with modified polar group and methyl substitution, and reiterated the role of sterol tilt as a key parameter regarding its effect on lipid membranes. An inverse relationship between θ and the ordering effects of a given sterol has been verified in subsequent studies, for diverse molecules such as intrinsically[13,14] or extrinsically[15,16] fluorescent sterols, 25-hydroxycholesterol,[17] cholesteryl hemisuccinate,[18] or β-sitosterol.[19]

While a direct relationship between sterol tilt and ordering capability appears to be clear, it should be recognized that the tilt itself depends on the sterol structure, and numerous types of chemical modifications affect sterol orientation within membranes,[20] as evident from the above examples. Sterol tilt itself is also influenced by the overall order of the membrane, which in turn depends on the phospholipid composition and sterol content as well as on the structure of the latter. Therefore, one has to be careful not to simply designate reduced sterol tilt as the direct cause for increased ordering, but to seek and characterize molecular determinants that influence both sterol orientation and their effect on membrane properties. Along these lines, a multivariate analysis of the relationship between the sterol structure and the resulting effects on membrane physical properties revealed that the most important determinants in this respect are, in decreasing order, the presence of an 8–10 carbon C17 isoalkyl side-chain (in opposition to polar groups or a shorter, 3–7 carbon chain), a hydroxyl group at C3 (in contrast to a keto group at this position) and a C5–C6 double bond (rather than a C4–C5 double bond).[21]

The latter study highlights the importance of an aliphatic chain of adequate length for optimal molecular packing with membrane phospholipids. In previous work, it was usually assumed that van der Waals interactions between the planar, fused ring system (particularly the smooth α-face) of cholesterol and saturated fatty acyl chains give rise to the favorable interaction of cholesterol with (saturated) phospholipid chains.[22,23] Interestingly, two recent experimental studies highlighted that the iso-branched cholesterol side chain plays a crucial role in various elementary membrane properties and accounts for 40–60% of the experimentally observed lipid condensation induced by cholesterol.[24,25] In a systematic study, the length of the iso-branched aliphatic side chain of cholesterol was altered, yielding a profound impact on basic membrane properties. Interestingly, membrane properties such as lipid condensation, lateral lipid diffusion, membrane permeability, and domain organization of lipids and transmembrane membrane protein segments appeared to be optimized for native cholesterol with the octanoyl sidechain providing a perfect length match with the phospholipids of the bilayer.

Atomistic MD simulations constitute a powerful method for the characterization of lipid membrane systems on an atomistic level[26] and, in particular, a very useful tool to investigate the behaviour of sterols in lipid bilayers complementary to experimental techniques (for reviews, see ref. 12, 27 and 28). Because

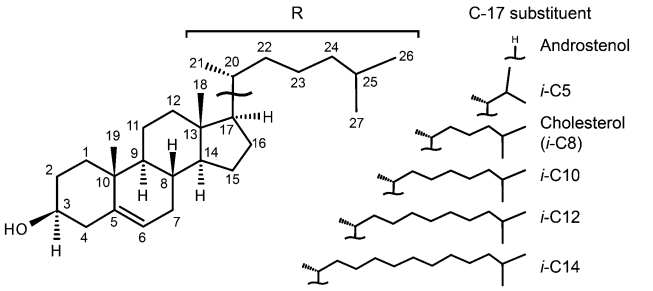

Fig. 1 Structure and atom numbering for the series of sterols with iso-branched side chains of varying lengths studied in this work.

MD simulations enable simultaneous and independent monitoring of the structural and dynamic features of sterol and phospholipid molecules, they can be used to characterize sterol location, orientation and dynamics, as well as the extent of perturbation they induce on the phospholipid matrix. In this work, we employ atomistic MD to study the above-mentioned series of sterols with an iso-branched alkyl chain at C17 of varying chain lengths. The compounds addressed provide side chains bearing 0 (i-C0, androstenol), 5 (i-C5), 8 (i-C8, cholesterol), 10 (i-C10), 12 (i-C12), or 14 (i-C14) carbon atoms (see Fig. 1 for sterol structure and atom numbering). Two types of simulations were carried out. In the first, a liquid crystalline bilayer of 1-palmitoyl-2-oleoyl-*sn*-*glycero*-3-phosphocholine (POPC) was simulated in the presence of only two sterol molecules (one in each 128-POPC bilayer leaflet). This intended to study local effects of the sterol on the properties of the phospholipid molecules located in its immediate surroundings. In a second set of simulations, the bilayer models contained a biologically relevant and substantially larger (20 mol%) fraction of sterol molecules. This ensured improved statistical relevance in the calculation of sterol properties, and also allowed for a more direct comparison with the aforementioned experimental data.[24] Consistent with the latter, in the present work we observe a maximal ordering effect for intermediate sterol chain lengths.

Simulation details

All simulations and analyses were carried out using the GROMACS 4.5 package.[29–31] The GROMACS force field (which is based on the GROMOS87 force field,[32] with modifications as detailed elsewhere[33–37]) was used to describe all the interactions, with the following adaptations. The united-atom (UA) topology of the POPC molecule, based on the 1,2-dipalmitoyl-*sn*-*glycero*-3-phosphatidylcholine (DPPC) description by Berger *et al.*,[38] and a POPC bilayer coordinate file were retrieved from Dr Peter Tieleman's group webpage.[39] The topology of POPC was then adapted to take into account the changed parameters for the double bond in the *sn*-2 acyl chain, as described elsewhere.[40,41] The UA structure and topology of cholesterol were adapted from that of Höltje *et al.*[42] (available for download at the GROMACS webpage[43]) by changing the molecule types from CH2/CH3 to LP2/LP3 to avoid overcondensation of the bilayer, as previously suggested,[44,45] and successfully tested by us.[46] Parameterizations of the other sterols were adapted from that

of cholesterol by removing/adding the appropriate number of methylene groups from/to each chain, for androstenol and i-C5, or the other sterols, respectively. Water was modeled with the simple point charge model.[47]

Bilayers containing either 128 POPC molecules or 128 POPC molecules and two molecules of each sterol (*i.e.*, 64 POPC and one sterol per leaflet) were assembled and hydrated with excess water (>30 H_2O per lipid).[48] For the other set of simulations, systems containing 96 POPC and 24 sterol molecules (corresponding to 20 mol% of the respective sterol) were also assembled and simulated. All sterols were inserted with hydroxyl groups facing the lipid/water interface and the sterol long axis normal to the bilayer plane. These initial configurations underwent an energy minimization (steepest descent) followed by a short run of 100 ps (1 fs time step; remaining parameters as described for the production run) and a 100 ns (for systems with no or two sterol molecules) or 300 ns (for systems with 20 mol% sterol) production simulation under the *NPT* ensemble and periodic boundary conditions, using Berendsen coupling schemes[49] for both pressure (semi-isotropic, 1.0 bar, 1.0 ps coupling time) and temperature (298.15 K, 0.1 ps coupling time). Bond length constraint algorithms SETTLE (water bonds)[50] and LINCS (other bonds)[51] allowed the use of a 2 fs time step. Cut-offs for both Coulomb and van der Waals interactions were set at 1.0 nm, while long-range electrostatics were conducted by the particle mesh Ewald method.[52]

Analysis used the final 80 ns (systems with none or two sterol molecules) or 200 ns (systems with 20 mol% sterol) of each production simulation, unless stated otherwise. Error estimates were obtained using the block method described by Flyvbjerg and Petersen.[53] For visualization of structures and trajectories, Visual Molecular Dynamics software (University of Illinois) was used.[54]

Results and discussion

Areas per lipid and bilayer thickness

Average cross-sectional areas per lipid molecule were evaluated by dividing the instant box area by the number of phospholipid molecules in each monolayer, 64 in the systems with none or two sterol molecules, and 48 in those containing 20 mol% sterol. This approach was carried out also in the latter case of mixtures of two major components for two reasons: (i) analysis of binary systems is more complicated, and more advanced approaches are needed;[55–59] and (ii) our objective was solely to verify convergence of the simulations and to compare the values obtained for the different sterols in the series, using all the same procedure.[60,61] Fig. S1 and S2 (ESI†) show the time variations of area per phospholipid in the systems with none or two sterol molecules as well as 20 mol% sterol, respectively. From these plots, it is apparent that equilibration of this parameter is generally achieved after 20 ns for the systems with none or two sterol molecules and 100 ns for those containing 20 mol% sterol, justifying our choices of time range used for analysis. The final structures of all simulations are depicted in Fig. S3 (none or two sterol molecules) and S4 (20 mol% sterol) (ESI†).

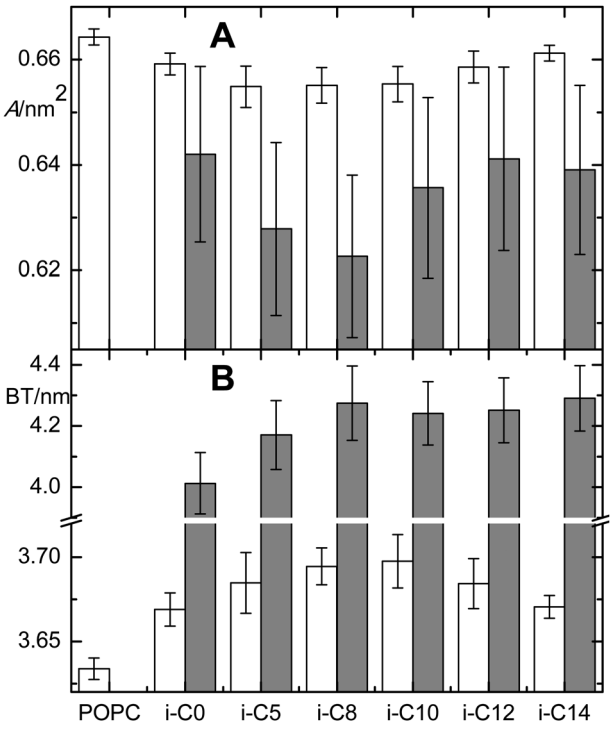

Fig. 2 (A) Average area per phospholipid *A* and (B) bilayer thickness BT for POPC bilayers containing none or two sterol molecules (white bars) or 20 mol% sterol (grey bars).

Fig. 2A displays the average areas per phospholipid in the membrane. The value obtained for pure POPC, $A = (0.664 \pm 0.002)$ nm^2, agrees well with published experimental (0.65 nm^2, T = 298 K;[62] 0.64 nm^2, T = 298 K;[63] and 0.68 nm^2, T = 303 K (ref. 64)) and simulation data (0.655 nm^2, T = 300 K;[65] 0.68 nm^2, T = 310 K;[66] 0.652 nm^2, T = 310 K (ref. 67)). Insertion of sterol molecules induces a decrease in the average area per phospholipid, which is referred to as condensation. Although this is a subtle effect, a U-shaped variation is visible along the series in agreement with experimental results,[24] with minimal values $A = (0.655 \pm 0.004)$ nm^2 obtained for intermediate chain length (i-C5, cholesterol, i-C10). This trend is echoed in the systems with larger sterol content. As expected, the bilayer thickness (calculated as the average difference between the transverse locations of the POPC P atoms in opposing leaflets) shows a largely inverse dependence on the sterol chain length (Fig. 2B), with a clear maximum for intermediate chain lengths in the simulations with two sterol molecules (white bars). On the other hand, in the simulations of POPC membranes containing 20 mol% sterol, the U shape is less pronounced and a plateau for sterol alkyl chains longer than that of cholesterol is observed.

Transverse location of POPC and sterol atoms

Fig. 3 shows the average transverse locations $\langle z \rangle$ of selected POPC and sterol atoms, relative to the bilayer midplane (z = 0). Along the series, the positions of the POPC head group/glycerol

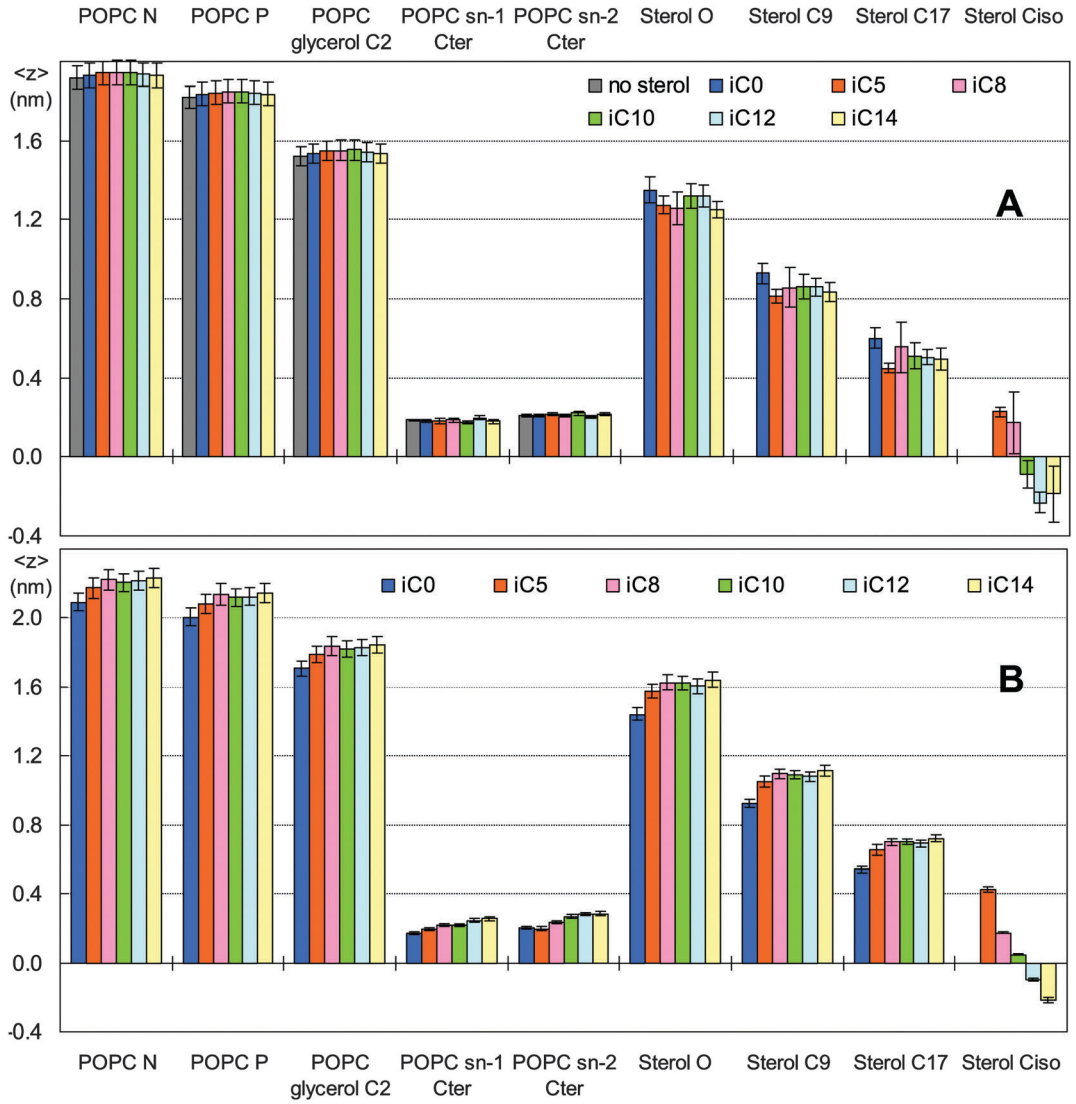

Fig. 3 Average transverse position $\langle z \rangle$ of specific POPC and sterol atoms in the simulations of systems containing none or two sterol molecules (A) and 20 mol% sterol (B). Cter designates the terminal methyl groups of the POPC acyl chains. Ciso denotes the CH group to which the two terminal methyl groups of the sterol alkyl chain are attached (*e.g.*, C25 for cholesterol, and correspondingly for the other sterols). See Fig. 1 for sterol atom numbering.

atoms display the same kind of variations (U-shaped for two sterol molecules, plateau for the longer-chained derivatives in the 20 mol% sterol systems) already apparent in the bilayer thickness profiles of Fig. 2B. The same applies to the position of the sterol oxygen atom and ring system carbon atoms C9 and C17 in the 20 mol% sterol systems (Fig. 3B). In particular, the former is consistently located ~0.2–0.25 nm below the POPC glycerol C2 atom, near the ester/carbonyl atoms of the phospholipid. No trends are apparent in the position of the corresponding sterol atoms in the systems illustrated in Fig. 3A, probably because of the very small number of sampled molecules.

Regarding the positions of the atoms located near the end of the POPC acyl/sterol alkyl chains, some interesting results are observed. In the systems with two sterol molecules, the locations of the terminal POPC acyl chain atoms are essentially invariant. However, the corresponding atoms in the 20 mol% sterol systems show a slight but steady variation, becoming progressively more distant from the bilayer center as the sterol alkyl chain length is increased. For example, for the POPC *sn*-2 terminal atom, $\langle z \rangle$ = (0.20 ± 0.01) nm for POPC/20 mol% androstenol, compared to $\langle z \rangle$ = (0.28 ± 0.01) nm for POPC/20 mol% i-C14.

Concomitantly, the sterol alkyl chain end atoms display progressively deeper average locations as the number of carbon atoms in the side chain increases. Among all studied sterols, native cholesterol is the one for which the positions of sterol Ciso (here defined as the CH group to which the two terminal methyl groups of the sterol alkyl chain are attached) match more closely the terminal atoms of POPC. The terminal alkyl chain atoms of i-C10, i-C12 and i-C14 have deeper average locations, in most cases with $\langle z \rangle < 0$. In other words, the chain end atoms of these sterols are predominantly protruding into the opposing leaflet. This interdigitation of alkyl or acyl chains of long-tailed solutes has been observed previously in MD simulation studies.[68–70]

For the most part, these effects are also apparent on the mass density profiles along the bilayer normal, depicted in Fig. S5 and S6 (ESI†) for the systems with none or two sterol molecules and 20 mol% sterol, respectively. Lengthening of the sterol alkyl chain produces an increase in sterol mass density near the centre of the bilayer, most visibly in the systems containing 20 mol% sterol. In turn, this leads to an augmented overall density in the centre of the bilayer. While the overall density at $z = 0$ is $\sim$605–610 kg m^{-3} for i-C5 and cholesterol, it increases to 630 kg m^{-3} for i-C10 and reaches $\sim$640–642 kg m^{-3} for i-C12 and i-C14. In this way, the above described slight separation of the POPC methyl atoms from the bilayer geometrical centre is possibly a consequence of the gradual occupation of this region with sterol alkyl chain atoms. As the system density becomes very high, the POPC acyl chain atoms become located further from the bilayer midplane, to provide room for the sterol atoms. This is a possible reason for the invariance of bilayer thickness from cholesterol to i-C14, despite the increase in the average area per phospholipid (Fig. 2, grey bars).

Curiously, for the systems containing two sterol molecules, Ciso of i-C12 protrudes more into the opposing leaflet when compared to the corresponding atom of i-C14. This is an indication that the sterol alkyl chain of the latter bends to avoid excessive penetration into the other monolayer, an effect which can be observed in the top molecule of the i-C14 final snapshot of Fig. S4 (ESI†). This led us to investigate the dependence of the transverse distance between the Ciso and C17 atoms (the latter being the sterol ring system atom to which the alkyl chain is attached, Fig. 1) on the alkyl chain length. A linear variation implies that the average sterol chain tilt remains constant along the series, whereas a sublinear dependence would indicate tilting of the chain or bending of its terminal segments. It can be seen that in the systems containing two sterol molecules (Fig. 4A), the plot is linear (albeit affected by uncertainty stemming from the small number of sampled molecules) up to i-C12, with a slope of (0.080 $\pm$ 0.018) nm per bond typical for that observed for lipids in fluid bilayers. This means that the chains of these molecules have comparable order to those of POPC. Despite i-C10 and i-C12 penetrating the opposing leaflet, this occurs with little resistance from the molecules of the opposing leaflet, and does not induce significant bending of the sterol chain. However, this is not the case for i-C14, whose chain is bent and does not penetrate the opposing leaflet any further than that of i-C12. On the other hand, for the systems containing 20 mol% sterol (Fig. 4B), the plot is now linear only up to (and including) cholesterol (slope = (0.105 $\pm$ 0.044) nm per bond, a value consistent with increased bilayer order; the large slope uncertainty merely reflects the fact that only three points were used). For the systems containing 20 mol% sterol, cholesterol is the molecule which leads to optimal matching between the sterol and the lipid chain. Longer chains than that of cholesterol imply a fraction of interdigitated configurations, but now these are much more impeded than in POPC alone, probably because of the increased membrane rigidity (for example, $\langle z \rangle$(Ciso) of i-C10 is now >0, whereas it was <0 in the corresponding two-sterol system).

Sterol tilt and the POPC acyl chain order

The extent of membrane ordering induced by the different sterols as a function of the sterol alkyl chain length, is of particular interest to this study, namely its relationship with sterol tilt. The sterol long axis was defined as the vector uniting the C16 and C3 ring system atoms (see Fig. 1). Fig. 5A shows the angular distributions of the long axis tilt relative to the bilayer normal, whereas the average tilts are depicted in Fig. 5B for the different sterols in the 20 mol% sterol systems. All sterols present very similar tilt distributions, although, on close inspection, those of cholesterol and i-C14 appear to be slightly narrower than the others. This is reflected in lower average values for these sterols, as shown in Fig. 5B. The dependence of the average tilt angle on the sterol chain length is parallel to that of area per phospholipid (Fig. 2A), characterized by a U-shaped profile with a minimum for cholesterol, and further decreases from i-C12 to i-C14. However, it must be emphasized that differences between sterols are not statistically significant. Tilt distributions and average values from the simulations with two sterol molecules displayed no discernible variation trends, probably because of the poor statistics arising from the sampling of only two molecules (not shown).

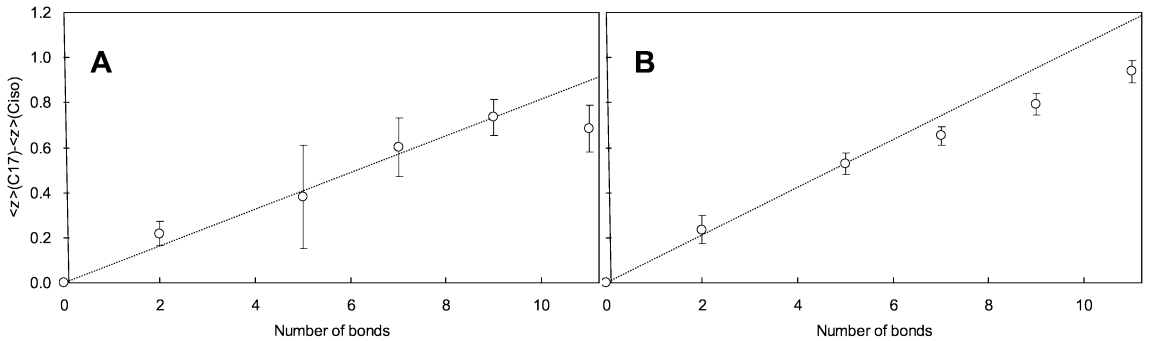

Fig. 4 Difference between the average transverse locations of sterol C17 and Ciso atoms as a function of the sterol alkyl chain length for the two sterol molecules (A) and 20 mol% sterol (B) systems. The dotted lines represent the linear fits to the points between androstenol and i-C12 in (A), and to those between androstenol and cholesterol in (B).

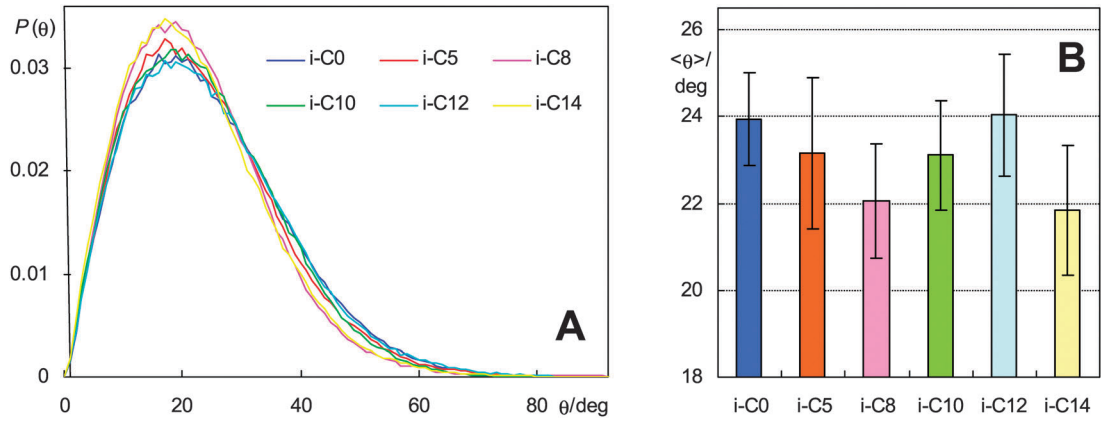

Fig. 5 Probability density functions $P(\theta)$ of the angle between the sterol long axis and the bilayer normal for POPC membranes containing 20 mol% sterol (A), and average values of these distributions (B).

Because the ring system is the same for all studied sterols, the slight variations observed in the sterol tilt distributions are probably related to differences in the sterol alkyl chain, namely their order along the bilayer normal. It seems plausible that sterol species whose alkyl chains are more ordered on average feature ring systems with less orientational freedom and lower average tilts. We calculated deuterium order parameters, S_{CD},[71] according to

$$S_{CD} = (3\langle\cos^2\theta\rangle - 1)/2 \quad (1)$$

where θ is the angle between a C–D bond and the bilayer normal, and the brackets denote averaging over time and C–D bonds. In our simulations, using a united atom force field, deuterium positions were constructed from the neighboring carbons assuming ideal geometries. $-S_{CD}$ can vary between 0.5 (full order along the bilayer normal) and -0.25 (full order along the bilayer plane), whereas $S_{CD} = 0$ denotes isotropic orientation.

Fig. 6 shows the order parameter profiles along the sterol alkyl chains in the 20 mol% sterol systems. In this plot, C20 corresponds to the first atom in the chain, and Ciso is the last atom for which an order parameter is calculated. Although S_{CD} inequivalence for the two hydrogen atoms has been reported in cholesterol for C24[72] and also for other methylene groups in the cholesterol side chain,[73] this difference cannot be resolved when calculating using the above described method. Therefore, the order parameters corresponding to these positions should be viewed as average values. Looking at the different profiles, the trend is very similar for most sterols (because i-C5 has a very short chain, it stands apart from the longer-chained sterols). The last atom in each curve (Ciso) has always a lower order parameter than expected from the other atoms in each curve. Discounting this atom, it can be seen that the profiles of cholesterol and i-C14 lie above those of i-C10 and i-C12, which correlates with the former lower average ring tilts compared to those of the latter. Sterol chain atoms below position 8 in Fig. 6 (between Ciso of i-C10 and i-C12) have average transverse location below the bilayer midplane (see Fig. 3B), and correspondingly low order parameter values, denoting a large degree of orientation randomization.

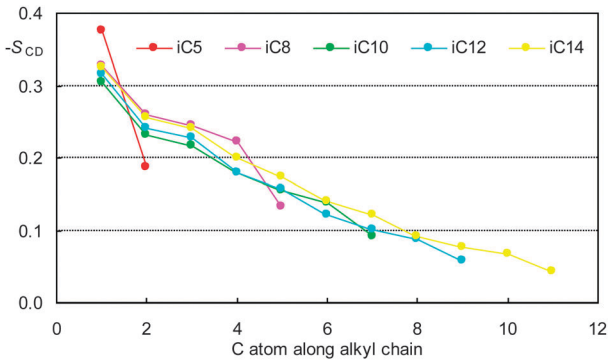

Fig. 6 Deuterium order parameter profiles of the sterol alkyl chains in the 20 mol% sterol systems.

The trends observed in the sterol ring tilts and chain order profiles are expected to be reflected on the order of the phospholipid acyl chains. Fig. 7 depicts the calculated $|S_{CD}|$ profiles of POPC in the presence of 20 mol% sterol derived from the MD simulations, while the corresponding averages over all segments are shown in Fig. 8. The results obtained in the absence of any sterol agree closely with both experimental (*e.g.*, ref. 45, 74 and 75) and simulated (*e.g.*, ref. 45, 65 and 67) profiles for pure POPC. It is clear that inclusion of all sterols leads to an increase in order compared to pure POPC. However, the extent of this increase varies noticeably across the different sterol species. Echoing the trends observed for other properties, a maximal ordering effect is observed for cholesterol (for which the calculated curves agree well with published experimental and simulated profiles[45]), whereas androstenol is clearly the least efficient species at ordering the phospholipid acyl chains.

The *sn*-1 chain averages plotted in Fig. 8A may be compared to the experimental data of Scheidt *et al.*,[24] obtained both in POPC and DPPC fluid lipid matrices (Fig. 8B). The calculated values are systematically higher than the experimental data for POPC by $\sim$0.05 units (they are actually closer to the data obtained in DPPC). This difference could arise from a number of reasons, including the lack of contribution of the C16 atom (the one for which $-S_{CD}$ is the lowest) in our calculation,

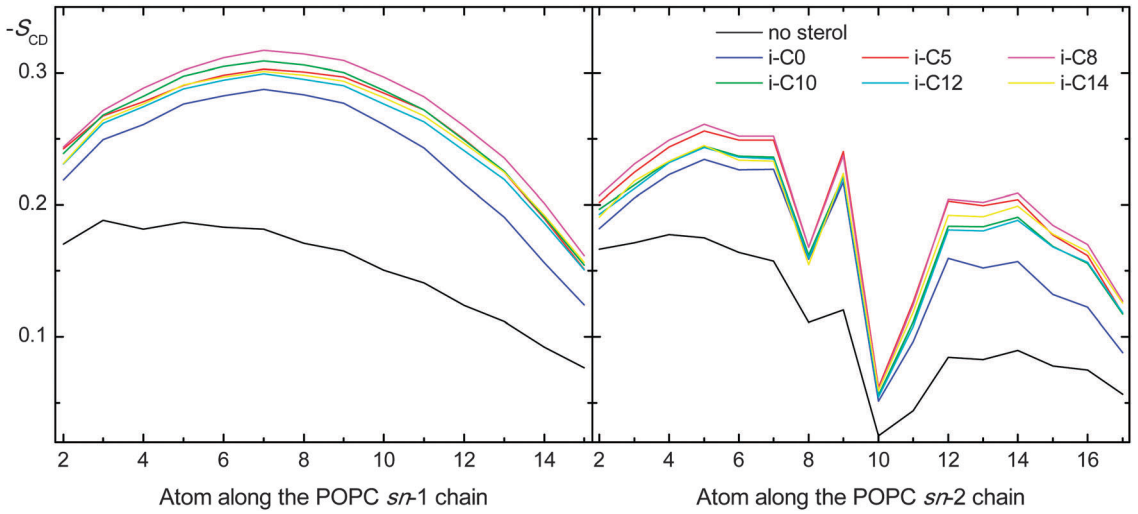

Fig. 7 Deuterium order parameter profiles of POPC acyl chains in the absence and presence (20 mol%) of the different sterols.

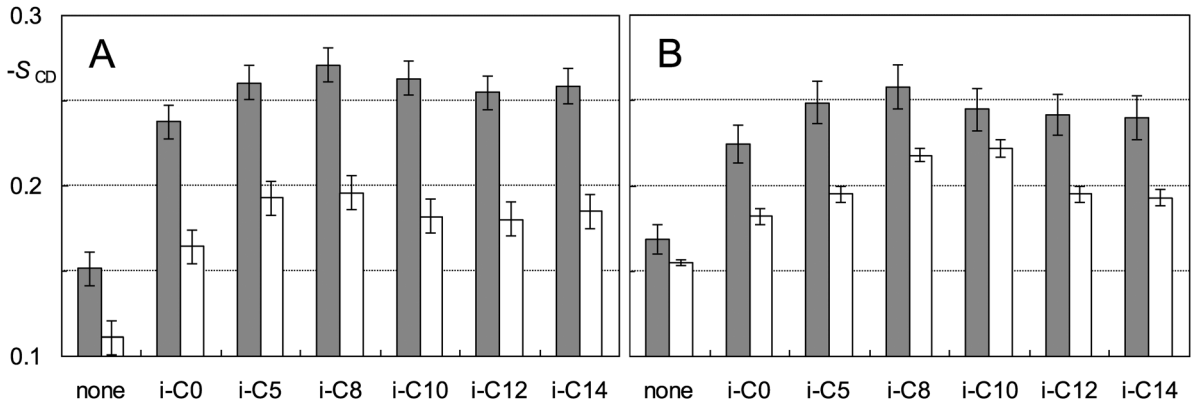

Fig. 8 (A) Calculated deuterium order parameters of POPC, averaged across C2–C15 of the *sn*-1 chain (grey bars) and C2–C17 of the *sn*-2 chain (white bars), in the absence and in the presence of 20 mol% of the respective sterol. (B) Experimental average order parameters of DPPC-d_{62} membranes (grey bars) and POPC-d_{31} membranes (white bars) in the absence and in the presence of 20 mol% of each sterol.[24]

incomplete equivalence between the simulated system and the samples prepared for the NMR experiments, or force field limitations. However, and most encouragingly, the trends of variation of the calculated and experimental data for the alkyl chain length agree very closely, both pointing to the maximal ordering effect for intermediate chain length, as well as much decreased ordering for androstenol, which has the same ring system as cholesterol, but lacks the aliphatic chain.

We now turn our attention to the simulations containing two sterol molecules. Fig. 9A–C show the order parameter profiles of the POPC *sn*-1 chain for different ranges of distance *R* to the sterol molecule within the same bilayer leaflet, while panels D to F display the respective averages over the chain atomic segments. An increase in the overall order parameters of the POPC is also observed in these systems (Fig. 9C and F), although it is understandably much smaller than in the bilayers containing 20 mol% sterol. However, these simulations are ideally suited for studying sterol-induced local effects on neighboring POPC chains, and provide information which is complementary to that of the systems containing 20 mol% sterol. Fig. 9A shows that although androstenol manages to exert some ordering on the top segments of neighboring POPC chains, it actually reduces the order parameter of the lower POPC atoms. This is unsurprising, because the absence of a chain leaves a void underneath the androstenol ring system, which tends to be occupied by the neighboring POPC chains (which become tilted in the process, leading to diminished order parameter values). On the other hand, cholesterol and the longer-chained sterols display comparable ordering effects on nearby POPC acyl chains. Although there is a maximum observed for cholesterol and i-C10, the differences to i-C12 and i-C14 are not significant. The behavior of i-C5 is intermediate between those of androstenol and cholesterol. Although it manages to increase order of all neighboring POPC acyl chain atoms (insignificantly so nearer the end, as expected), it does so less efficiently than the longer-chained sterols.

As we[70] and others[65,67,76,77] have recently demonstrated, small cations such as Na^+ bind to the ester/carbonyl atoms of

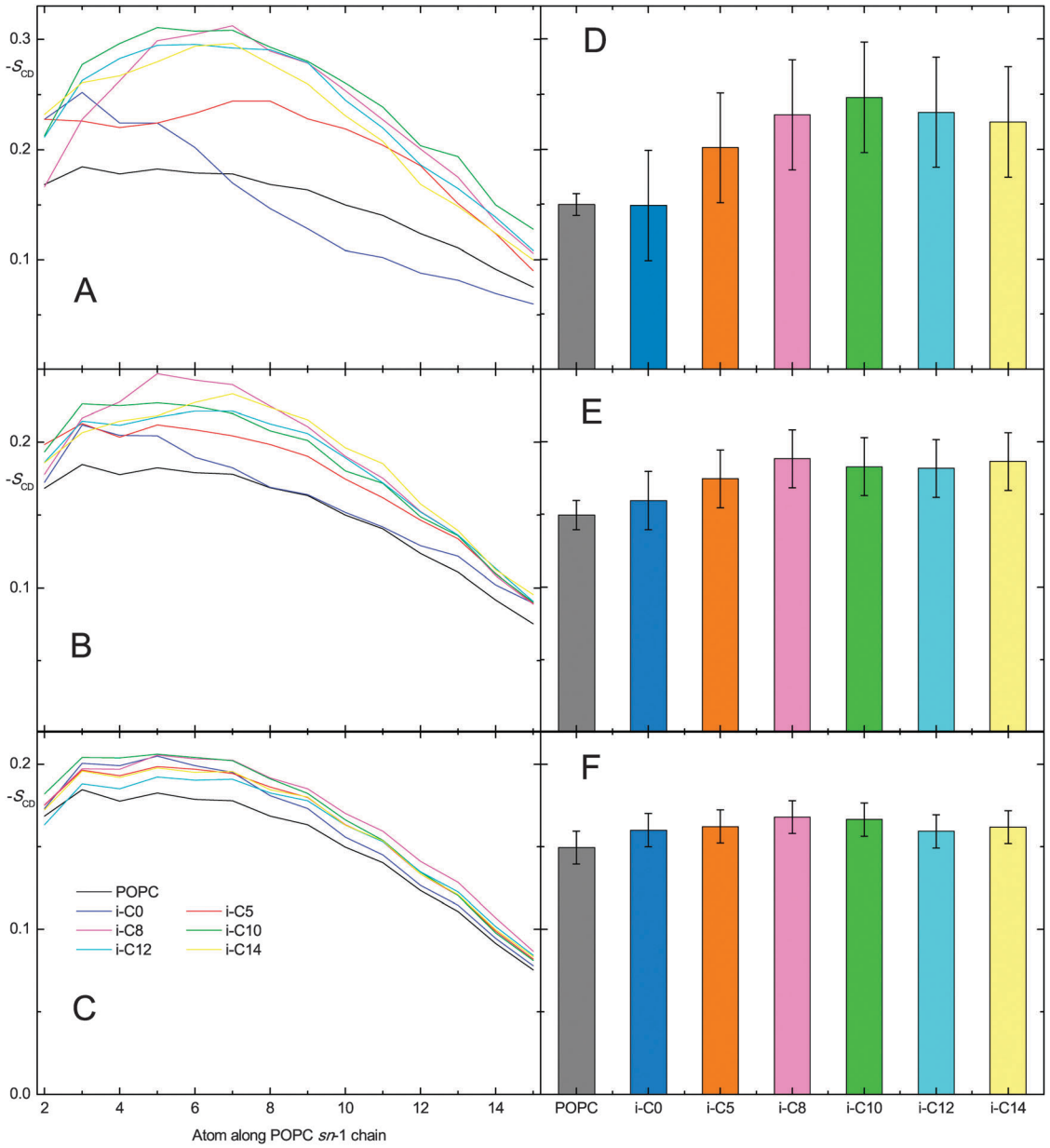

Fig. 9 POPC *sn*-1 order parameter profiles (left panels) calculated in the two sterol simulations, and corresponding averages along the chain (right panels), for different ranges of distance R to the closest sterol molecule in the same bilayer leaflet (A and D: $R < 0.6$ nm; B and E: 0.6 nm $< R <$ 1.2 nm; C and F: all chains).

phospholipids, inducing a slight enhancement of the lipid order (whereas common counter ions such as Cl^- remain firmly in the aqueous phase and do not affect the lipids). Although we have not included ions in these simulations, we expect that the addition of a salt such as NaCl would lead to a systematic ordering effect, identical for all sterols along the series, and therefore all comparative conclusions of this study would be unchanged. This was observed in the homologous series of fluorescent NBD-diC_nPE phospholipids (n = 4, 6, 8, 10, 12, 14, 16, 18),[70] in which, because of the anionic nature of the lipid probes, sodium ions are added to the system. In this report, Na^+ induced a slight general overall ordering effect, without masking a systematic variation along the series (with maximal ordering for the optimally matching chains of NBD-diC_{16}PE).

Interactions with POPC and water

Although the variations are very slight and within the statistical uncertainty, the data of Fig. 7 and 8 indicate that different sterols may interact distinctly with the two acyl chains of POPC. For example, while cholesterol is the sterol which induces a larger average order increase in both acyl chains, it is immediately followed by i-C10 in *sn*-1, but by i-C5 in *sn*-2. Several literature studies have addressed the question of whether cholesterol interacts preferably with saturated phospholipid acyl chains over unsaturated ones (reviewed in ref. 12 and 28). For example, it has

been experimentally verified that cholesterol is segregated in a flat orientation inside the middle of bilayers composed of polyunsaturated fatty acid chains.[78,79] On the other hand, apparently 5 mol% of saturated phospholipid 1,2-dimyristoyl-*sn-glycero*-3-phosphocholine (DMPC) can revert the upright orientation of cholesterol in polyunsaturated 1,2-diarachidonoyl-*sn-glycero*-3-phosphocholine, whereas a much higher content of POPC (50 mol%) is required for this effect.[80] This suggests that cholesterol has affinity for saturated hydrocarbon chains, aversion for polyunsaturated fatty acid chains, and an intermediate behavior regarding phospholipids bearing one saturated and one unsaturated chain, such as POPC. To gain more insight into this question, we calculated radial distribution functions (RDFs) of POPC *sn*-1 (saturated) and *sn*-2 acyl (monounsaturated) chain atoms around each sterol in the 20 mol% systems, which are shown in Fig. 10.

In all cases, a very small peak can be observed at $R \sim 0.25$ nm, reflecting H-bonding of sterol OH to the glycerol/carbonyl O atoms. Because of its location near the glycerol/carbonyl region of the bilayer (Fig. 3), the sterol hydroxyl group is prone to act as a H-bond donor to water, POPC phosphate or (predominantly) POPC ester/carbonyl oxygen atoms. On the other hand, because of water penetration into this region (see Fig. S5, ESI†), the sterol oxygen atom can also act as a H-bond acceptor from water OH groups. The relative frequencies of instantaneous configurations displaying H-bonds of both types are shown in Fig. S7 (ESI†). Intermolecular sterol–sterol H-bonds are virtually absent, having only residual occurrence. These results are very similar for the different sterols, and no definite trends can be observed upon varying the sterol chain length. On close inspection of Fig. 10, it becomes apparent that this short-distance interaction is consistently stronger for the *sn*-2 chain, possibly because of steric reasons (the *sn*-2 chain atoms have slightly shallower locations than the corresponding ones of *sn*-1), and/or due to slightly more electronegative character of *sn*-2 O in the phospholipid model used here.[38]

Possibly of larger interest in Fig. 10 is the region $0.3 \text{ nm} < R < 1.2$ nm, which contains the nearest- and second-nearest neighboring shells of POPC molecules around each sterol. For intermediate chain length, namely cholesterol and i-C10, a preferential interaction with *sn*-1 is apparent, as the corresponding peak is noticeably higher than that of the *sn*-2 chain. This preference is much decreased (if existent at all) for i-C12 and i-C14. Regarding i-C5 and (especially) androstenol, if anything, there is a preference for the *sn*-2 chain. In the case of cholesterol at least, it is tempting to relate the increased *sn*-1 $g(R)$ to the above commented affinity for saturated fatty acid chains. From our calculations, it appears that the existence of an aliphatic chain of adequate length is determinant for this preferential interaction.

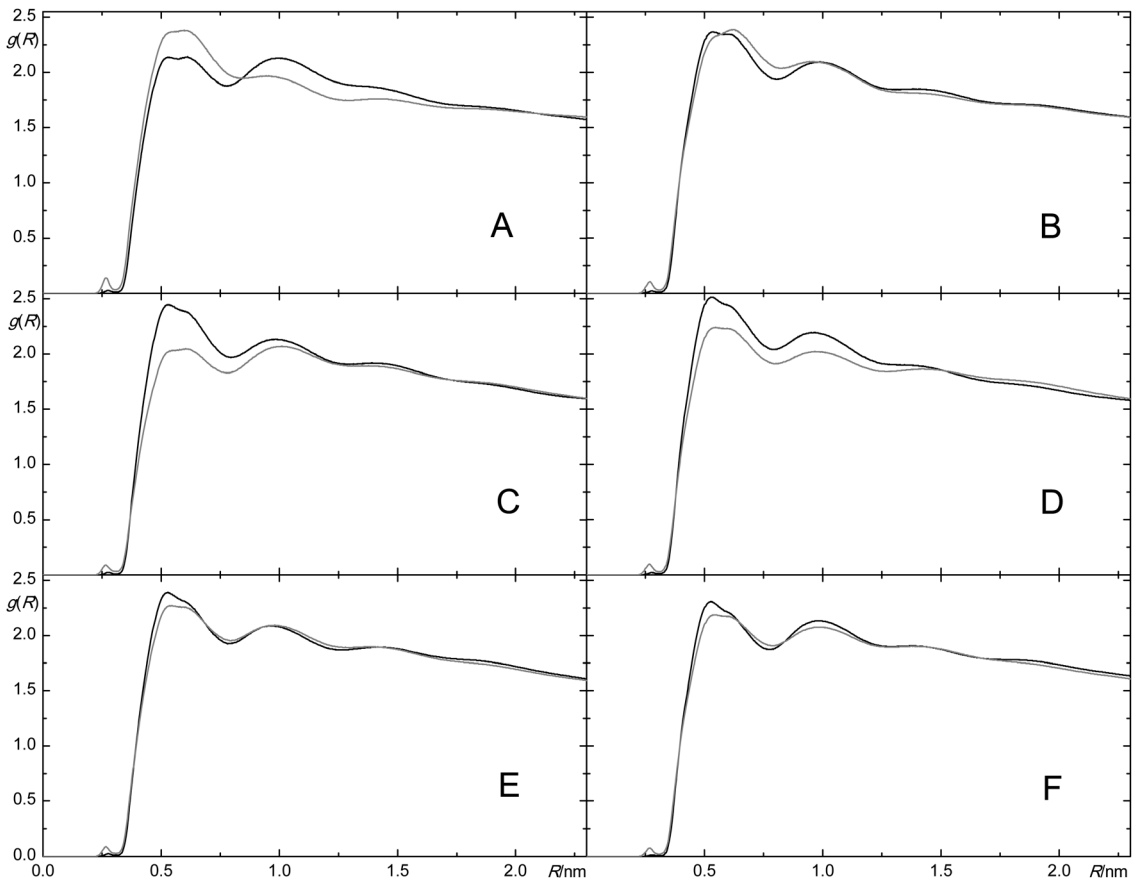

Fig. 10 Radial distribution functions $g(R)$ of *sn*-1 (black lines) and *sn*-2 (grey lines) POPC acyl chain atoms around sterol molecules in the 20 mol% simulations. From (A–F): androstenol, i-C5, cholesterol, i-C10, i-C12, i-C14.

Dynamical properties

We also addressed the dynamics of sterol and lipid motions. In order to study the rotational dynamics of the sterols, a rotational autocorrelation function $C(t)$ was calculated, as defined below:

$$C(t) = \langle P_2(\cos\theta(\xi))\rangle \quad (2)$$

where $\theta(\xi)$ is the angle between the sterol long axis at times ξ and $t + \xi$, and $P_2(x) = (3x^2 - 1)/2$ is the second Legendre polynomial. Averaging is performed both over ξ and sterol molecules. The rotational autocorrelation functions calculated for the systems containing 20 mol% sterol are shown in Fig. 11. For all systems, finite residual values of $C(t)$ are observed at long times, that is, these functions appear to have finite limits as $t \to \infty$. This is common for solutes embedded in lipid bilayers, and may arise from hindered rotational motion, such as arising from a "wobbling-in-cone"-type rotation.[81] In accordance with this hypothesis, during the course of our simulations, no translocation of sterol molecules (which would require complete molecular rotation) to the opposite leaflet occurred, and, as apparent from the tilt distributions of Fig. 5A, tilt angles $\theta > 50^\circ$ are infrequent.

It can be appreciated that cholesterol and i-C14 are the sterols whose axes rotate the slowest, followed by i-C5, i-C10 and i-C12. For these three sterols, the curves are similar, especially at shorter times (which is the most statistically meaningful region of these plots). Androstenol rotates fastest of all studied derivatives. Thus, these results correlate with the order parameter and area/phospholipid values, as sterol rotation is slowest in the most ordered/condensed systems.

Lateral diffusion coefficients D were calculated from the two-dimensional mean squared displacement (MSD), using the Einstein relation

$$D = \frac{1}{4}\lim_{t\to\infty}\frac{\mathrm{dMSD}(t)}{\mathrm{d}t} \quad (3)$$

In turn, MSD is defined by

$$\mathrm{MSD}(t) = \left\langle \|\vec{r}_i(t + t_0) - \vec{r}_i(t_0)\|^2 \right\rangle \quad (4)$$

where $\vec{r}_i$ is the (x, y) position of the centre of mass of molecule i of a given species, and the averaging is carried out over all molecules of this kind and time origins t_0. To eliminate noise due to fluctuations in the centre of mass of each monolayer, all MSD analyses were carried out using trajectories with fixed centre of mass of one of the monolayers, and the final result is averaged over the two leaflets. Fig. S8 (ESI†) shows MSD for POPC and sterols for the systems containing 20 mol% of the latter, while the corresponding D values (obtained from fits to the linear region of the MSD plots) are given in Fig. 12.

The significance of MSD plots and accurate calculation of lateral diffusion in membranes remains, to a great extent, a controversial problem. It depends largely on the available time window.[26,82] Sampling problems are more important in lateral diffusion than in some other properties, because it involves large-scale motions of whole molecules rather than limited range/segmental motions (like those involved in lipid acyl chains or probe long axis orientation). For relatively short times, lipid diffusion (as perceived by MSD variation) is mainly due to conformational changes of the hydrocarbon chains rather than diffusion of the entire molecule,[26] and therefore its meaning and its relationship to experimental observables are somewhat questionable. For these reasons, we will refrain from a quantitative discussion of absolute D values, and will focus on trends of variation across the studied series instead.

In this context, some features can be identified in the data of Fig. 12: (i) phospholipid and sterols have generally similar diffusion coefficients (less so for the longer-chained sterols, see discussion below); (ii) both phospholipid and sterol diffusion coefficients present a minimum for intermediate chain length; and (iii) the increase of sterol lateral diffusion coefficient (compared to cholesterol) is more pronounced for the longer-chained sterols (and actually non-significant for shorter-chained sterols). All these features can also be identified in the experimental data obtained in DPPC : sterol 1 : 1 mixtures at 50 °C.[24] In our simulations, the variation of POPC D is approximately inverse of that of the average order parameters (Fig. 8), and a similar variation is observed for the lateral diffusion coefficients of the shorter-chained sterols. However, unlike the data reported by Scheidt *et al.*,[24] our calculated i-C14 D value is significantly higher than that of the phospholipid in the same system. The probable reason why the lateral diffusion coefficients are unexpectedly high for the longer-chained sterols in our calculations is that they are computed taking into account all atomic displacements.

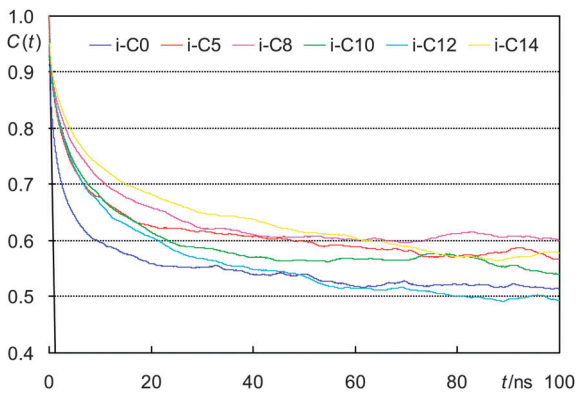

Fig. 11 Rotational autocorrelation functions $C(t)$ (see the text for definition) of the sterol long axis in POPC membranes containing 20 mol% sterol.

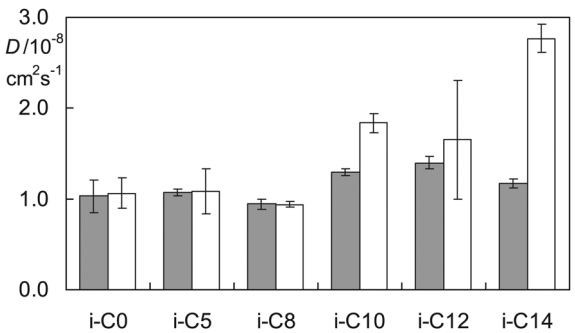

Fig. 12 Lateral diffusion coefficients D of POPC (grey bars) and sterol (white bars) in the systems with 20 mol% sterol.

All sterols share the same ring system, but, for longer tails, increasingly more sterol atoms are located in the alkyl chain, and therefore the relative weight of the latter in the calculation of D is increased. Because these atoms are located in the most disordered and fluid region of the bilayer, lengthening of the chain leads to a sizeable increase in the calculated D. Accordingly, if MSD plots were calculated taking solely into account the ring system of each sterol, a significant decrease (by 35%) would be obtained for the i-C14 D value (not shown). From these data, one can infer that interdigitation of the end chain segments of these sterols does not present much hindrance to their lateral diffusion. To understand this result, one may use the atomic positions of Fig. 3B to reason that, because the average position of i-C14 the Ciso atom, albeit negative (−0.22 nm) and thus beyond the bilayer midplane, is still not inside the positions of the terminal atoms of the POPC terminal methyl atoms of the opposing leaflet ($z \sim -0.25$ to -0.28 nm). Therefore, the degree of protrusion of sterol alkyl chains into regions occupied by lipids in the opposing leaflet is probably limited, and the longer-chained sterols tend to bend their tails near the end (as illustrated in some of the configurations displayed in Fig. S4, ESI†).

Concluding remarks

In this work, we used atomistic MD simulations to characterize in detail a homologous series of cholesterol derivatives with varying alkyl side chain lengths, inserted inside POPC bilayers. For some of the calculated parameters, we found agreement with trends of variation reported in a recent experimental study,[24] namely the lipid order parameters $|S_{CD}|$ show maximal values for intermediate chain length, while lipid and sterol lateral diffusion coefficients show an inverse chain length dependence to that of $|S_{CD}|$.

More importantly, the data reported here allowed us to gain new important insights. It was found that the tail ends of the longer-chained sterols have a location beyond the center plane of the membrane and into the opposing bilayer leaflet. To minimize unfavorable overlap with the acyl chains of lipids in the opposing monolayer, the end segments of the chains of these sterols are bent, and, for 20 mol% sterol containing membranes, POPC acyl chain atoms move further away from the bilayer midplane, to provide room for these sterol atoms. Even though a noticeable extent of chain ordering occurs for intermediate chain lengths, sterol tilt distributions are similar for all derivatives. This emphasizes the importance of an alkyl chain of adequate length as a determinant of sterol ability to modify membrane properties. This condition is met for sterols of intermediate side chain lengths, notably cholesterol. For these sterols, a preferential interaction with the saturated *sn*-1 chain of POPC (over the unsaturated *sn*-2 chain) was detected. Importantly, this preferential association with saturated lipid chains, previously suggested as a possible driving force for the formation of cholesterol-induced membrane domains such as lipid rafts,[5,8,83,84] is attenuated for both shorter- and longer-chained sterols.

Acknowledgements

L. M. S. L. acknowledges the Laboratory for Advanced Computing at University of Coimbra for computing resources, and funding by Fundação para a Ciência e Tecnologia (Portugal), project references PTDC/BBB-BQB/2661/2012 and UID/QUI/00313/2013. J. R. R. acknowledges the Max Planck Institute for Colloids and Interfaces for funding under the IMPRS on Multiscale Bio-Systems.

Notes and references

1 S. R. Shaikh, J. J. Kinnun, X. Leng, J. A. Williams and S. R. Wassall, *Biochim. Biophys. Acta*, 2015, **1848**, 211–219.
2 O. G. Mouritsen and M. J. Zuckermann, *Lipids*, 2004, **39**, 1101–1113.
3 E. London, *Biochim. Biophys. Acta*, 2005, **1746**, 203–220.
4 M. F. Brown, *Biochemistry*, 2012, **51**, 9782–9795.
5 M. L. Frazier, J. R. Wright, A. Pokorny and P. F. F. Almeida, *Biophys. J.*, 2007, **92**, 2422–2433.
6 A. Tsamaloukas, H. Szadkowska and H. Heerklotz, *J. Phys.: Condens. Matter*, 2006, **18**, S1125–S1138.
7 D. Huster, K. Arnold and K. Gawrisch, *Biochemistry*, 1998, **37**, 17299–17308.
8 P. F. F. Almeida, A. Pokorny and A. Hinderliter, *Biochim. Biophys. Acta*, 2005, **1720**, 1–13.
9 E. Oldfield, M. Meadows, D. Rice and R. Jacobs, *Biochemistry*, 1978, **17**, 2727–2740.
10 J. Aittoniemi, T. Róg, P. Niemelä, M. Pasenkiewicz-Gierula, M. Karttunen and I. Vattulainen, *J. Phys. Chem. B*, 2006, **110**, 25562–25564.
11 G. Khelashvili and D. Harries, *Chem. Phys. Lipids*, 2013, **169**, 113–123.
12 T. Róg, M. Pasenkiewicz-Gierula, I. Vattulainen and M. Karttunen, *Biochim. Biophys. Acta*, 2009, **1788**, 97–121.
13 J. R. Robalo, A. M. T. Martins do Canto, A. J. Palace Carvalho, J. P. Prates Ramalho and L. M. S. Loura, *J. Phys. Chem. B*, 2013, **117**, 5806–5819.
14 M. Pourmousa, T. Róg, R. Mikkeli, I. Vattulainen, L. M. Solanko, D. Wüstner, N. H. List, J. Kongsted and M. Karttunen, *J. Phys. Chem. B*, 2014, **118**, 7345–7357.
15 M. Hölttä-Vuori, R.-L. Uronen, J. Repakova, E. Salonen, I. Vattulainen, P. Panula, Z. Li, R. Bittman and E. Ikonen, *Traffic*, 2008, **9**, 1839–1849.
16 J. R. Robalo, J. P. Prates Ramalho and L. M. S. Loura, *J. Phys. Chem. B*, 2013, **117**, 13731–13742.
17 B. N. Olsen, P. H. Schlesinger and N. A. Baker, *J. Am. Chem. Soc.*, 2009, **131**, 4854–4865.
18 W. Kulig, P. Jurkiewicz, A. Olżyńska, J. Tynkkynen, M. Javanainen, M. Manna, T. Róg, M. Hof, I. Vattulainen and P. Jungwirth, *Biochim. Biophys. Acta*, 2015, **1848**, 422–432.
19 Z. E. Hughes and R. L. Mancera, *Soft Matter*, 2013, **9**, 2920–2935.
20 D. A. Mannock, R. N. A. H. Lewis, T. P. W. McMullen and R. N. McElhaney, *Chem. Phys. Lipids*, 2010, **163**, 403–448.
21 J. J. Wenz, *Biochim. Biophys. Acta*, 2012, **1818**, 896–906.
22 M. A. Davies, H. F. Schuster, J. W. Brauner and R. Mendelsohn, *Biochemistry*, 1990, **29**, 4368–4373.

23 G. Orädd, V. Shahedi and G. Lindblom, *Biochim. Biophys. Acta*, 2009, **1788**, 1762–1771.
24 H. A. Scheidt, T. Meyer, J. Nikolaus, D. J. Baek, I. Haralampiev, L. Thomas, R. Bittman, A. Herrmann, P. Müller and D. Huster, *Angew. Chem., Int. Ed.*, 2013, **52**, 12848–12851.
25 T. Meyer, D. J. Baek, R. Bittman, I. Haralampiev, P. Muller, A. Herrmann, D. Huster and H. A. Scheidt, *Chem. Phys. Lipids*, 2014, **184**, 1–6.
26 A. P. Lyubartsev and A. L. Rabinovich, *Soft Matter*, 2011, **7**, 25–39.
27 M. L. Berkowitz, *Biochim. Biophys. Acta*, 2009, **1788**, 86–96.
28 T. Róg and I. Vattulainen, *Chem. Phys. Lipids*, 2014, **184**, 82–104.
29 H. J. C. Berendsen, D. van der Spoel and R. van Drunen, *Comput. Phys. Commun.*, 1995, **91**, 43–56.
30 D. van der Spoel, E. Lindhal, B. Hess, G. Groenhof, A. Mark and H. J. C. Berendsen, *J. Comput. Chem.*, 2005, **26**, 1701–1718.
31 B. Hess, C. Kutzner, D. van der Spoel and E. Lindahl, *J. Chem. Theory Comput.*, 2008, **4**, 435–447.
32 W. F. van Gunsteren and H. J. C. Berendsen, *Gromos-87 manual*, Biomos BV, Groningen, The Netherlands, 1987.
33 A. R. van Buuren, S. J. Marrink and H. J. C. Berendsen, *J. Phys. Chem.*, 1993, **97**, 9206–9212.
34 A. E. Mark, S. P. van Helden, P. E. Smith, L. H. M. Janssen and W. F. van Gunsteren, *J. Am. Chem. Soc.*, 1994, **116**, 6293–6302.
35 W. L. Jorgensen, J. Chandrasekhar, J. D. Madura, R. W. Impey and M. L. Klein, *J. Chem. Phys.*, 1983, **79**, 926–935.
36 A. R. van Buuren and H. J. C. Berendsen, *Biopolymers*, 1993, **33**, 1159–1166.
37 H. Liu, F. Müller-Plathe and W. F. van Gunsteren, *J. Am. Chem. Soc.*, 1995, **117**, 4363–4366.
38 O. Berger, O. Edholm and F. Jähnig, *Biophys. J.*, 1997, **72**, 2002–2013.
39 http://wcm.ucalgary.ca/tieleman/downloads, accessed May 2015.
40 M. Bachar, P. Brunelle, D. P Tieleman and A. Rauk, *J. Phys. Chem. B*, 2004, **108**, 7170–7179.
41 H. Martinez-Seara, T. Róg, M. Karttunen, R. Reigada and I. Vattulainen, *J. Chem. Phys.*, 2008, **129**, 105103.
42 M. Höltje, T. Förster, B. Brandt, T. Engels, W. von Rybinski and H. Höltje, *Biochim. Biophys. Acta*, 2001, **1511**, 156–167.
43 http://www.gromacs.org/index.php?title=Download_%26_Installation/User_contributions/Molecule_topologies, accessed May 2015.
44 D. P. Tieleman, J. L. MacCallum, W. L. Ash, C. Kandt, Z. T. Xu and L. Monticelli, *J. Phys.: Condens. Matter*, 2006, **18**, S1221–S1234.
45 T. M. Ferreira, F. Coreta-Gomes, O. H. S. Ollila, M. J. Moreno, W. L. C. Vaz and D. Topgaard, *Phys. Chem. Chem. Phys.*, 2013, **15**, 1976–1989.
46 A. M. T. M. do Canto, P. D. Santos, J. Martins and L. M. S. Loura, *Colloids Surf., A*, 2015, **480**, 296–306.
47 H. J. C. Berendsen, J. P. M. Postma, W. F. Van Gunsteren and J. Hermans, in *Intermolecular Forces*, ed. B. Pullman, Reidel, Dordrecht, The Netherlands, 1981, pp. 331–342.
48 K. Murzyn, T. Róg, G. Jezierski, Y. Takaoka and M. Pasenkiewicz-Gierula, *Biophys. J.*, 2001, **81**, 170–183.
49 H. J. C. Berendsen, J. P. M. Postma, W. F. van Gunsteren, A. DiNola and J. R. Haak, *J. Chem. Phys.*, 1984, **81**, 3684–3690.
50 S. Miyamoto and P. A. Kollman, *J. Comput. Chem.*, 1992, **13**, 952–962.
51 B. Hess, H. Bekker, H. J. C. Berendsen and J. G. E. M. Fraaije, *J. Comput. Chem.*, 1997, **18**, 1463–1472.
52 U. Essmann, L. Perera, M. L. Berkowitz, T. Darden, H. Lee and L. G. Pedersen, *J. Chem. Phys.*, 1995, **103**, 8577–8593.
53 H. Flyvbjerg and H. G. Petersen, *J. Chem. Phys.*, 1989, **91**, 461–466.
54 W. Humphrey, A. Dalke and K. Schulten, VMD – Visual Molecular Dynamics, *J. Mol. Graphics*, 1996, **14**, 33–38.
55 S. W. Chiu, E. Jakobsson, R. J. Mashl and H. L. Scott, *Biophys. J.*, 2002, **83**, 1842–1853.
56 C. Hofsäß, E. Lindahl and O. Edholm, *Biophys. J.*, 2003, **84**, 2192–2206.
57 S. A. Pandit, S. Vasudevan, S. W. Chiu, R. J. Mashl, E. Jakobsson and H. L. Scott, *Biophys. J.*, 2004, **87**, 1092–1100.
58 O. Edholm and J. F. Nagle, *Biophys. J.*, 2005, **89**, 1827–1832.
59 M. Alwarawrah, J. Dai and J. Huang, *J. Phys. Chem. B*, 2010, **114**, 7516–7523.
60 T. Róg, M. Pasenkiewicz-Gierula, I. Vattulainen and M. Karttunen, *Biophys. J.*, 2007, **92**, 3346–3357.
61 M. Franová, J. Repáková, P. Capková, J. M. Holopainen and I. Vattulainen, *J. Phys. Chem. B*, 2010, **114**, 2704–2711.
62 G. Lantzsch, H. Binder, H. Heerklotz, M. Wendling and G. Klose, *Biophys. Chem.*, 1996, **58**, 289–302.
63 B. Konig, U. Dietrich and G. Klose, *Langmuir*, 1997, **13**, 525–532.
64 N. Kučerka, S. Tristram-Nagle and J. F. Nagle, *J. Membr. Biol.*, 2005, **208**, 193–202.
65 R. A. Bockmann, A. Hac, T. Heimburg and H. Grubmüller, *Biophys. J.*, 2003, **85**, 1647–1655.
66 S. Ollila, M. T. Hyvönen and I. Vattulainen, *J. Phys. Chem. B*, 2007, **111**, 3139–3150.
67 A. Gurtovenko and I. Vattulainen, *J. Phys. Chem. B*, 2008, **112**, 1953–1962.
68 R. R. Gullapalli, M. C. Demirel and P. J. Butler, *Phys. Chem. Chem. Phys.*, 2008, **10**, 3548–3560.
69 H. A. L. Filipe, M. J. Moreno and L. M. S. Loura, *J. Phys. Chem. B*, 2011, **115**, 10109–10119.
70 H. A. L. Filipe, L. S. Santos, J. P. Prates Ramalho, M. J. Moreno and L. M. S. Loura, *Phys. Chem. Chem. Phys.*, 2015, **17**, 20066–20079.
71 J. Seelig, *Q. Rev. Biophys.*, 1977, **10**, 353–418.
72 E. J. Dufourc, E. J. Parish, S. Chitrakorn and C. P. Smith, *Biochemistry*, 1984, **23**, 6062–6071.
73 A. Vogel and D. Huster, unpublished results.
74 J. Seelig and N. Waespe-Šarčević, *Biochemistry*, 1978, **17**, 3310–3315.
75 G. Klose, B. Mädler, H. Schäfer and K. Schneider, *J. Phys. Chem. B*, 1999, **103**, 3022–3029.
76 S. K. Kandasamy and R. G. Larson, *Biochim. Biophys. Acta*, 2006, **1758**, 1274–1284.

77 G. Pabst, A. Hodzic, J. Štrancar, S. Danner, M. Rappolt and P. Laggner, *Biophys. J.*, 2007, **93**, 2688–2696.
78 T. A. Harroun, J. Katsaras and S. R. Wassall, *Biochemistry*, 2006, **45**, 1227–1233.
79 T. A. Harroun, J. Katsaras and S. R. Wassall, *Biochemistry*, 2008, **47**, 7090–7096.
80 N. Kucerka, D. Marquard, T. A. Harroun, M.-P. Nieh, S. R. Wassall, D. H. de Jong, L. V. Schafer, S. J. Marrink and J. Katsaras, *Biochemistry*, 2010, **49**, 7485–7493.
81 K. Kinosita, S. Kawato and A. Ikegami, *Biophys. J.*, 1977, **20**, 289–305.
82 M. Javanainen, H. Hammaren, L. Monticelli, J.-H. Jeon, M. S. Miettinen, H. Martinez-Seara, R. Metzler and I. Vattulainen, *Faraday Discuss.*, 2013, **161**, 397–417.
83 A. Bunge, P. Müller, M. Stöckl, A. Herrmann and D. Huster, *Biophys. J.*, 2008, **94**, 2680–2690.
84 T. Bartels, R. S. Lankalapalli, R. Bittman, K. Beyer and M. F. Brown, *J. Am. Chem. Soc.*, 2008, **130**, 14521–14532.

